

Polarization Properties of Low Energy Amplitude  
for  $\pi N \rightarrow \pi\pi N$  ReactionA.A. Bolokhov<sup>1</sup>, V.A. Kozhevnikov<sup>1</sup>, S.G. Sherman<sup>2</sup> and D.N. Tatarkin<sup>1</sup><sup>1</sup> *Sankt-Petersburg State University,  
Sankt-Petersburg, 198904, Russia*<sup>2</sup> *St. Petersburg Institute for Nuclear Physics,  
Sankt-Petersburg, 188350, Russia***Abstract**

The theoretical study of cross sections for polarized-target measurements of  $\pi N \rightarrow \pi\pi N$  reactions gives evidence that the interplay between the strong contribution from OPE mechanism and the one from isobar exchanges, which is equally strong within isobar half-widths energy region, must result in nontrivial polarization phenomena. The Monte-Carlo simulations for asymmetries in  $\pi^- p^\uparrow \rightarrow \pi^- \pi^+ n$  reaction at  $P_{\text{Lab}} = 360$  MeV/c with the use of theoretical amplitudes found as solutions for unpolarized data at  $P_{\text{Lab}} < 500$  MeV/c provide confirmations for significant effect. The effect is capable to discriminate between the OPE and isobar exchanges and it is sensitive to the OPE parameters in question. This leads to the conclusion that the decisive  $\pi N \rightarrow \pi\pi N$  analysis, aiming at determination of  $\pi\pi$ -scattering lengths, must combine both unpolarized data and polarization information. The appropriate measurements are shown to be feasible at the already existing CHAOS spectrometer.

PACS number(s): 13.75.-n, 13.75.Gx, 13.75.Lb

Sankt-Petersburg  
1998

# 1 Introduction

The  $\pi N \rightarrow \pi\pi N$  reaction is considered to be an essential source of information on the  $\pi\pi$  scattering. The values of  $\pi\pi$ -scattering lengths can give restrictions for values of the effective low-energy parameters of QCD obtained within the framework of ChPT (Chiral Perturbation Theory) which was formulated by Gasser and Leutwiller in [1, 2] following Weinberg's ideas [3, 4, 5]. The appearance of GChPT (Generalized ChPT) scheme [6] enhanced the interest to the  $\pi\pi$  interaction because of difference in the predicted  $\pi\pi$ -scattering lengths with that given by ChPT.

A review on the experimental opportunities for obtaining information on the  $\pi\pi$  interaction and the discussion of the status of modern experiments planned to test the ChPT predictions might be found in the talks [7, 8] by Počanić. The investigations of  $\pi N \rightarrow \pi\pi N$  reactions are pronounced to be capable to discriminate between the ChPT and GChPT models for low-energy manifestations of QCD. Meanwhile the most recent attempts [9, 10, 11, 12, 13] of analysis of the  $\pi N \rightarrow \pi\pi N$  data did not provide the necessary accuracy.

One must recall that there are three methods for the  $\pi N \rightarrow \pi\pi N$  data treatment applicable at the low energies. These are:

1. The approach by Olsson and Turner [14], presenting the formulae that express the  $\pi\pi$ -scattering lengths  $a_0^{I=0}$ ,  $a_0^{I=2}$  in terms of the threshold characteristics of the  $\pi N \rightarrow \pi\pi N$  reactions;
2. The model-independent Chew–Low extrapolation procedure by Goebel, Chew and Low [15];
3. The method of determination of the OPE parameters directly in the physical region of the reaction by Oset and Vicente–Vacas [16]; it is based on the  $\pi N \rightarrow \pi\pi N$  phenomenological amplitude accounting for exchanges of the appropriate resonances.

Due to simplicity of the approach **1** and the statistical reliability of the total-cross-section data it operates with, the approach gained a broad scale of applications when the modern data started to appear in the close-to-threshold energy region [17, 18, 19, 20], [21], [22], [23].

Recently the heavy baryon approximation was used to derive corrections to the Olsson–Turner formulae [24, 25]. The progress of the later theoretical calculations of the  $\pi N \rightarrow \pi\pi N$  amplitude within the same framework [26, 27, 28] resulted in conclusion that uncertainty in isobar interactions prevented from accurate determination of the isospin-zero scattering length  $a_0^{I=0}$ . Finally, it was stated in [29] that the result for  $a_0^{I=0}$  of the analysis [25] cannot be trusted.

The conclusion that  $a_0^{I=2}$  acquired minor perturbations from isobars was made with the help of rather simple model of  $\pi\pi NN^{(*)}$  and  $\pi\pi N\Delta$  interactions. The investigations of various contributions to threshold amplitudes performed in the paper [30] with more general isobar interactions

raised doubts in the result for  $a_0^{I=2}$  as well. Moreover, it was found that two independent threshold amplitudes for  $\pi N \rightarrow \pi\pi N$  reactions collected noticeable contributions from the  $O(k^4)$  parameters of the OPE graph. The determination of four  $\pi\pi$  characteristics by virtue of only two  $\pi N \rightarrow \pi\pi N$  threshold experimental quantities becomes a model-dependent problem that requires additional theoretical and experimental information.

The most recent applications of the Chew–Low method **2** to the near-threshold data provided the  $\pi\pi$ -scattering lengths with the almost perfect accuracy [10, 12]. However, because of making use of assumptions about  $\pi N \rightarrow \pi\pi N$  amplitude at zero momentum transfer, this method suffers from unknown systematic errors which cannot be estimated within the approach. The known problems of applications of the method at higher energies are discussed in [31, 32]. The analysis of properties of the extrapolation procedure in the near-threshold region is made in [30] in the framework of the approach **3**. The theoretical amplitudes were used to show that the strong influence of isobars in this region can result in inapplicability to synthetic data of both linear and quadratic extrapolations. The reported failure of the Chew–Low analysis of data for the channel  $\pi^+ p \rightarrow \pi^+ \pi^+ n$  [12] might serve as an indirect evidence for disregard of other successful extrapolations since there might be observed a contradiction with the previous statement that the  $I_{\pi\pi} = 2$  channel is less perturbed near threshold by isobar contributions [26, 27, 28, 29], see the previous paragraph; this definitely requires a separate explanation. The announced in the talk [12] long awaited analysis of real data of the best quality obtained at the CHAOS device [33] must become a checkpoint for low-energy applications of the discussed method.

The relativistic version of the approach **3** was used recently [9] to treat the large set of the near-threshold data on total cross sections and 1-D distributions in the energy region  $300 \leq P_{\text{Lab}} \leq 500$  MeV/c. The phenomenological amplitude for the reaction  $\pi N \rightarrow \pi\pi N$ , taking into account the exchanges of  $\Delta$  and  $N^{(*)}$  along with the OPE mechanism and polynomial background derived with the account of isotopic, crossing,  $C$ ,  $P$  and  $T$  symmetries of strong interactions, was fitted to the experimental data. Though the parameters of OPE are found to be statistically significant, the  $\pi\pi$ -scattering lengths appear different in different solutions. The origin of difficulties is attributed to the influence of isobars. Eight parameters of  $\pi\pi N\Delta$  and  $\pi\pi NN^{(*)}$  interactions, being only weakly constrained by the widths of decays  $\Delta \rightarrow \pi\pi N$ ,  $N^{(*)} \rightarrow \pi\pi N$ , strongly correlate with the OPE parameters in question.

The common difficulty of the discussed methods originates from limitations to data of unpolarized measurements which cannot discriminate between contributions to different spin-structures of the reaction amplitude. Up to now the known polarization measurements of the  $\pi N \rightarrow \pi\pi N$

reactions had been performed at considerably higher energies, for example, at 5.98 GeV/c and 11.85 GeV/c [34] and at 17.2 GeV/c [35]. The analyses of the polarized data [36], [37] already proved such measurements to be detailed sources of information on the  $\pi\pi$  interaction.

The main goals of the present paper is to elaborate the theoretical framework for treating the polarization measurements of  $\pi N \rightarrow \pi\pi N$  reactions at low energies and to find out the suitable observables. We pay a separate attention for a study of the principal possibility to perform polarized  $\pi N \rightarrow \pi\pi N$  experiments at the already existing CHAOS spectrometer [33]. The primary goal is to ensure the solution of the urgent problem: the obtaining of the  $\pi\pi$ -scattering characteristics with the help of the solid bank of available  $\pi N \rightarrow \pi\pi N$  data and simple polarization measurements added.

We base upon the general properties of the  $\pi N \rightarrow \pi\pi N$  amplitude. It describes five charge channels in terms of only four isoscalar functions. Moreover, three of these functions are strongly restricted by crossing symmetry to only one independent function (see [38, 39, 40]). To take advantage of intimate relations between various channels we prefer to rely upon the crossing symmetry rather than the partial-wave expansion. Obviously, the approach **3** is assumed.

The paper is organized as follows. The content of sect. 2 reminds the structure of the  $\pi N \rightarrow \pi\pi N$  amplitude. Sect. 3 provides expressions necessary for calculations of cross sections in experiments with the polarized target. Sect. 4 is devoted to geometry of devices and analyzed asymmetries. It contains the results of modelling the experimental measurements with the use of various solutions found in the paper [9] for the  $\pi N \rightarrow \pi\pi N$  amplitude. The summary, the concluding remarks and the discussion of implementations are given in Conclusions.

## 2 General Structure of $\pi N \rightarrow \pi\pi N$ Amplitude

This short section introduces the basic formulae of the papers [40, 9].

We consider the reaction

$$\pi^a(k_1) + N_\alpha(p; \lambda_i) \rightarrow \pi^b(k_2) + \pi^c(k_3) + N_\beta(q; \lambda_f) , \quad (1)$$

where  $a, b, c = 1, 2, 3$  and  $\alpha, \beta = 1, 2$  are isotopic indices of pions and nucleons, respectively, and  $\lambda_i$  ( $\lambda_f$ ) are polarizations of initial (final) nucleons.

Separating the nucleon spinor wave functions from the reaction amplitude  $M_{\beta\alpha}^{abc}(\lambda_f; \lambda_i)$

$$M_{\beta\alpha}^{abc}(\lambda_f; \lambda_i) = \bar{u}(q; \lambda_f) \hat{M}_{\beta\alpha}^{abc}(i\gamma_5) u(p; \lambda_i) , \quad (2)$$

one can define the isoscalar amplitudes  $\hat{A}, \hat{B}, \hat{C}, \hat{D}$  by

$$\hat{M}_{\beta\alpha}^{abc} = \hat{A}\tau_{\beta\alpha}^a\delta^{bc} + \hat{B}\tau_{\beta\alpha}^b\delta^{ac} + \hat{C}\tau_{\beta\alpha}^c\delta^{ab} + \hat{D}i\epsilon^{abc}\delta_{\beta\alpha}, \quad (3)$$

$\tau^a$ ,  $a = 1, 2, 3$  being the nucleon–isospin generators. The amplitudes of five observable channels are related to  $A, B, C, D$  by

$$\begin{aligned} \hat{M}_{\{\pi^-p \rightarrow \pi^- \pi^+ n\}} &= \sqrt{2}/2 (\hat{A} + \hat{C}), \quad \hat{M}_{\{\pi^-p \rightarrow \pi^0 \pi^0 n\}} = 1/2 (\hat{A}), \\ \hat{M}_{\{\pi^-p \rightarrow \pi^- \pi^0 p\}} &= 1/2 (\hat{C} - 2\hat{D}), \quad \hat{M}_{\{\pi^+p \rightarrow \pi^+ \pi^0 p\}} = 1/2 (\hat{C} + 2\hat{D}), \\ \hat{M}_{\{\pi^+p \rightarrow \pi^+ \pi^+ n\}} &= 1/2 (\hat{B} + \hat{C}). \end{aligned} \quad (4)$$

To simplify the processing of cross sections, the statistical factors accounting for identical pions are inserted into these definitions. Below, we leave only the charges of the final pions in subscripts for the channels.

To decompose each isoscalar function  $\hat{A}, \hat{B}, \hat{C}, \hat{D}$  and each amplitude  $\hat{M}_X$ ,  $X = \{-+n\}, \{-0p\}, \{00n\}, \{++n\}, \{+0p\}$  into independent spinor form factors let us define the crossing–covariant complex combinations  $k = k_R + ik_I$ ,  $\bar{k} = k_R - ik_I$  of pion momenta

$$k = -k_1 + \epsilon k_2 + \bar{\epsilon} k_3, \quad \bar{k} = -k_1 + \bar{\epsilon} k_2 + \epsilon k_3, \quad (5)$$

$$k_R = -k_1 - (k_2 + k_3)/2, \quad k_I = \sqrt{3}(k_2 - k_3)/2, \quad (6)$$

where  $\epsilon \equiv \exp(2\pi i/3) = -1/2 + i\sqrt{3}/2$ ,  $\bar{\epsilon} = \epsilon^* = -1/2 - i\sqrt{3}/2$ . The decomposition reads

$$\begin{aligned} \hat{M}_X &= S_X + \bar{V}_X \hat{k} + V_X \hat{\bar{k}} + i/2 T_X [\hat{k}, \hat{\bar{k}}] \equiv \begin{pmatrix} S_X \\ \bar{V}_X \\ V_X \\ T_X \end{pmatrix}^T \cdot \begin{pmatrix} \hat{1} \\ \hat{k} \\ \hat{\bar{k}} \\ i/2[\hat{k}, \hat{\bar{k}}] \end{pmatrix}, \\ &(X = \{-+n\}, \{-0p\}, \{00n\}, \{++n\}, \{+0p\}). \end{aligned} \quad (7)$$

Since polarization phenomena are determined by the interference of real and imaginary parts of the amplitude, it is convenient to deal with combinations

$$S_X, \quad V_X^R \equiv (V_X + \bar{V}_X)/2, \quad V_X^I \equiv (V_X - \bar{V}_X)/(2i), \quad T_X, \quad (8)$$

which are shown to be approximately real in the energy region where unitarity corrections are small (see [39]). So we rewrite the decomposition (7) in the form:

$$\begin{aligned} \hat{M}_X &= \begin{pmatrix} S_X \\ V_X^R \\ V_X^I \\ T_X \end{pmatrix}^T \cdot \begin{pmatrix} \hat{1} \\ 2\hat{k}_R \\ 2\hat{k}_I \\ [\hat{k}_R, \hat{k}_I] \end{pmatrix}, \\ &(X = \{-+n\}, \{-0p\}, \{00n\}, \{++n\}, \{+0p\}). \end{aligned} \quad (9)$$

The matrix element  $\|M\|^2$  entering the unpolarized cross section is the sum over final polarizations and the average over initial ones. It is the quadratic form of the vector of spinor form factors  $(S_X, V_X^R, V_X^I, T_X)$ :

$$\begin{aligned} \|M_X\|^2 &\equiv 1/2 \sum_{\lambda_f, \lambda_i} \left[ \bar{u}(q; \lambda_f) \hat{M}_X(i\gamma_5) u(p; \lambda_i) \right] \left[ \bar{u}(q; \lambda_f) \hat{M}_X(i\gamma_5) u(p; \lambda_i) \right]^* \\ &= \begin{pmatrix} S_X \\ V_X^R \\ V_X^I \\ T_X \end{pmatrix}^T G_R \begin{pmatrix} S_X \\ V_X^R \\ V_X^I \\ T_X \end{pmatrix}^* = \begin{pmatrix} S_X \\ V_X^R \\ V_X^I \\ T_X \end{pmatrix}^\dagger G_R \begin{pmatrix} S_X \\ V_X^R \\ V_X^I \\ T_X \end{pmatrix}, \\ &\quad (X = \{-+n\}, \{-0p\}, \{00n\}, \{++n\}, \{+0p\}). \end{aligned} \quad (10)$$

The real hermitian matrix  $G_R$  is obtained by calculating the  $\gamma$ -matrix traces

$$G_R \equiv \frac{1}{2} \text{Sp} \left[ (\hat{q} + m) \begin{Bmatrix} \hat{1} \\ 2\hat{k}_R \\ 2\hat{k}_I \\ [\hat{k}_R, \hat{k}_I] \end{Bmatrix} (\hat{p} - m) \gamma_0 \begin{Bmatrix} \hat{1} \\ 2\hat{k}_R \\ 2\hat{k}_I \\ [\hat{k}_R, \hat{k}_I] \end{Bmatrix}^\dagger \gamma_0 \right]. \quad (11)$$

Its explicit expression will be given below, see eqs. (14).

### 3 Cross Section for Polarized–Target Measurements

The origin of strong correlations between parameters of OPE and isobar contributions, preventing from the accurate determination of the  $\pi\pi$ -scattering lengths in the unpolarized experiment, is obvious now. Only the specific combination of the competing contributions given by eq. (10) can be measured in such experiments. Bringing this matrix to the diagonal form one can realize that any diagonal amplitude can mimic the OPE one outside the region of isobar poles.

Though the measurement of the final polarization in the  $\pi N \rightarrow \pi\pi N$  reaction is implied by the design of the spectrometer AMPIR (see [41]), such measurements are hardly to be performed in the near future. Therefore, we consider the polarized–target experimental setup. For simplicity, we assume the ideal polarization. It is easy to generalize our results to the incomplete polarization due to the linear dependence of all asymmetries upon the polarization vector  $\mathbf{s}$ . Indeed, given nontrivial probabilities  $w_{\lambda_1}, w_{\lambda_2}$  ( $w_{\lambda_1} + w_{\lambda_2} = 1$ ) for the projection of the initial nucleon spin in the direction  $\mathbf{n}_s \equiv \mathbf{s}/|\mathbf{s}|$  to be  $\lambda_1 = 1/2, \lambda_2 = -1/2$ , respectively, any theoretical result for asymmetry must be derived with  $|\mathbf{s}| = w_s = 2w_{\lambda_1} - 1 = w_{\lambda_1} - w_{\lambda_2}$ . We set  $w_s = 1$  in calculations.

The matrix element  $\|M\|_s^2$  is now defined by

$$\|M_X\|_s^2 \equiv \sum_{\lambda_f} \left[ \bar{u}(q; \lambda_f) \hat{M}_X(i\gamma_5) u(p; \lambda_i) \right] \left[ \bar{u}(q; \lambda_f) \hat{M}_X(i\gamma_5) u(p; \lambda_i) \right]^*$$

$$\begin{aligned}
&= \begin{pmatrix} S_X \\ V_X^R \\ V_X^I \\ T_X \end{pmatrix}^T G \begin{pmatrix} S_X \\ V_X^R \\ V_X^I \\ T_X \end{pmatrix}^* = \begin{pmatrix} S_X \\ V_X^R \\ V_X^I \\ T_X \end{pmatrix}^\dagger G^* \begin{pmatrix} S_X \\ V_X^R \\ V_X^I \\ T_X \end{pmatrix}, \\
&(X = \{-+n\}, \{-0p\}, \{00n\}, \{++n\}, \{+0p\}).
\end{aligned} \tag{12}$$

The hermitian matrix  $G \equiv G_R + iG_I$  is given by

$$G \equiv \text{Sp} \left[ (\hat{q} + m_f) \begin{Bmatrix} \hat{1} \\ 2\hat{k}_R \\ 2\hat{k}_I \\ [\hat{k}_R, \hat{k}_I] \end{Bmatrix} (\hat{p} - m_i) \frac{1 + \gamma_5 \hat{s}}{2} \gamma_0 \begin{Bmatrix} \hat{1} \\ 2\hat{k}_R \\ 2\hat{k}_I \\ [\hat{k}_R, \hat{k}_I] \end{Bmatrix}^\dagger \gamma_0 \right], \tag{13}$$

where the polarization 4-vector  $s$  equals  $(0, \mathbf{s})$  in the rest frame of the initial nucleon.

The real part  $G_R$  of this matrix enters the unpolarized cross section (conf. eqs. (11) and (13)).

The imaginary part  $G_I$  is skew-symmetric. These matrices are explicitly given by

$$\begin{aligned}
G_R(1,1) &= 2(-m_i m_f + p \cdot q), \\
G_R(1,2) &= 4(-m_i q \cdot k_R + m_f p \cdot k_R), \\
G_R(1,3) &= 4(-m_i q \cdot k_I + m_f p \cdot k_I), \\
G_R(1,4) &= 4(-p \cdot k_R q \cdot k_I + q \cdot k_R p \cdot k_I), \\
G_R(2,2) &= 8(-m_i m_f k_R \cdot k_R - p \cdot q k_R \cdot k_R + 2p \cdot k_R q \cdot k_R), \\
G_R(2,3) &= 8(-m_i m_f k_R \cdot k_I - p \cdot q k_R \cdot k_I + p \cdot k_R q \cdot k_I \\
&\quad + q \cdot k_R p \cdot k_I), \\
G_R(2,4) &= 8(-m_i q \cdot k_R k_R \cdot k_I + m_i q \cdot k_I k_R \cdot k_R \\
&\quad - m_f p \cdot k_R k_R \cdot k_I + m_f p \cdot k_I k_R \cdot k_R), \\
G_R(3,3) &= 8(-m_i m_f k_I \cdot k_I - p \cdot q k_I \cdot k_I + 2p \cdot k_I q \cdot k_I), \\
G_R(3,4) &= 8(-m_i q \cdot k_R k_I \cdot k_I + m_i q \cdot k_I k_R \cdot k_I \\
&\quad - m_f p \cdot k_R k_I \cdot k_I + m_f p \cdot k_I k_R \cdot k_I), \\
G_R(4,4) &= 8(-m_i m_f k_R \cdot k_R k_I \cdot k_I + m_i m_f (k_R \cdot k_I)^2 \\
&\quad + p \cdot q k_R \cdot k_R k_I \cdot k_I - p \cdot q (k_R \cdot k_I)^2 \\
&\quad - 2p \cdot k_R q \cdot k_R k_I \cdot k_I + 2p \cdot k_R q \cdot k_I k_R \cdot k_I \\
&\quad + 2q \cdot k_R p \cdot k_I k_R \cdot k_I - 2p \cdot k_I q \cdot k_I k_R \cdot k_R),
\end{aligned} \tag{14}$$

$$G_I(1,2) = -4 \text{eps}[p, q, s, k_R],$$

$$\begin{aligned}
G_I(1, 3) &= -4 \text{eps}[p, q, s, k_I] , \\
G_I(1, 4) &= 4 (\text{eps}[p, s, k_R, k_I] m_f - \text{eps}[q, s, k_R, k_I] m_i) , \\
G_I(2, 3) &= 8 (\text{eps}[p, s, k_R, k_I] m_f + \text{eps}[q, s, k_R, k_I] m_i) , \\
G_I(2, 4) &= 8 (\text{eps}[p, q, s, k_R] k_R \cdot k_I - \text{eps}[p, q, s, k_I] k_R \cdot k_R \\
&\quad + 2 \text{eps}[p, q, k_R, k_I] s \cdot k_R + 2 \text{eps}[q, s, k_R, k_I] p \cdot k_R) , \\
G_I(3, 4) &= 8 (\text{eps}[p, q, s, k_R] k_I \cdot k_I - \text{eps}[p, q, s, k_I] k_R \cdot k_I \\
&\quad + 2 \text{eps}[p, q, k_R, k_I] s \cdot k_I + 2 \text{eps}[q, s, k_R, k_I] p \cdot k_I) , 
\end{aligned} \tag{15}$$

where the following notation

$$\text{eps}[x, y, u, v] \equiv \epsilon_{\mu\nu\rho\sigma} x^\mu y^\nu u^\rho v^\sigma$$

is used and nucleon masses  $m_i$ ,  $m_f$  are allowed to be different. Matrix elements in eqs. (15) are actually ordered according to their importance in the near-threshold region.

Let us now consider the fixed reaction channel and omit the channel's subscript in the notation for the vector  $M$  of form factors (8). The form factors  $V^R$ ,  $V^I$  are obtained by splitting off the real and imaginary parts in the cross-covariant momenta of the spinor structures  $\hat{k}$ ,  $\hat{\bar{k}}$ . The form factors themselves remain complex:  $V^R \equiv V_R^R + iV_I^R$ ,  $V^I \equiv V_R^I + iV_I^I$ . Consider the real and imaginary parts of the amplitude:

$$M_R \equiv \begin{pmatrix} S_R \\ V_R^R \\ V_R^I \\ T_R \end{pmatrix}, \quad M_I \equiv \begin{pmatrix} S_I \\ V_I^R \\ V_I^I \\ T_I \end{pmatrix}. \tag{16}$$

Then the matrix element (12) can be rewritten as

$$\|M\|_s^2 = M_R^T G_R M_R + M_I^T G_R M_I + 2M_R^T G_I M_I. \tag{17}$$

Here, the first two terms of the right-hand side give the unpolarized matrix element (10). The effect of polarization is provided by the third term.

Two conclusions can be immediately derived from this form and the above explicit expressions for matrices  $G_R$ ,  $G_I$ .

**1.** OPE contributes only to the spinor form factor  $S$  of the decompositions (7), (9). Hence, the validity of the assumption about the OPE dominance means that there cannot be any asymmetry in the reaction cross sections at the energies where the assumption holds.

**2.** It is necessary for polarization effect that both real and imaginary parts of the amplitude remain non-negligible. Fortunately, several partial waves are mixed up in the polarization term of



eq. (17). So the polarization effect must manifest itself in asymmetries of cross sections not only at the isobar poles ( $P_{\text{Lab}} \approx 500$  Mev/c for  $\Delta$  and  $P_{\text{Lab}} \approx 660$  Mev/c for  $N^{(*)}$ ) but well below due to the large widths of these resonances.

Rich kinematics of the considered reaction give rise to the abundance of possibilities for manifestation of polarization in the polarized-target experiments. There are five distinct structures entering the matrix  $G_I$  of eq. (17). These are

$$\text{eps}[p, q, s, k_R] = -3/2 \text{eps}[p, q, s, k_1] , \quad (18)$$

$$\text{eps}[p, q, s, k_I] , \quad (19)$$

$$\text{eps}[p, s, k_R, k_I] , \quad (20)$$

$$\text{eps}[q, s, k_R, k_I] , \quad (21)$$

$$\text{eps}[p, q, k_R, k_I] = -3\sqrt{3}/4 \text{eps}[p, q, k_1, k_2 - k_3] . \quad (22)$$

One finds that, depending on the relative strength of form factors (16), any of the above structures can govern the discussed effects. Four structures (18), (19), (20), (21), entering matrix elements  $G_I(1, 2)$ ,  $G_I(1, 3)$  and  $G_I(1, 4)$  related to OPE, are also present in the rest elements given by eqs. (15). At small  $\mathbf{q}$ ,  $\mathbf{k}_2$ ,  $\mathbf{k}_3$ , the terms (18), (19) are the most favourable ones for detecting OPE since extra factors at the same terms in  $G_I(2, 3)$ ,  $G_I(2, 4)$ ,  $G_I(3, 4)$  eliminate the effect when averaged. At the same time, there is the single term (22) which is specific to non-OPE contributions only. It can be “switched off” by  $(s \cdot k_R)$  factor since vector  $\mathbf{k}_R$  belongs to narrow backward cone at low energies. This phenomenon is a characteristic feature of non-OPE mechanisms.

Let two vectors  $\mathbf{x}$ ,  $\mathbf{y}$  determine the plane  $(\mathbf{x}, \mathbf{y})$ , separating “left” and “right” semi-spheres and  $\mathbf{z}$  be some third vector. Let  $\varphi_{\mathbf{z}}$  be its azimuthal angle in the plane which contains  $\mathbf{y}$  and is orthogonal to the plane  $(\mathbf{x}, \mathbf{y})$ . The asymmetry

$$A_{(\mathbf{x}, \mathbf{y})}(\varphi_{\mathbf{z}}) \equiv \frac{\sigma(\varphi_{\mathbf{z}}) - \sigma(-\varphi_{\mathbf{z}})}{\sigma(\varphi_{\mathbf{z}}) + \sigma(-\varphi_{\mathbf{z}})} \quad (23)$$

shows the relative value of the polarization term of eq. (17) with respect to unpolarized cross section. Obviously, several asymmetries must be observed to detect the influence of all above structures (18)–(22).

It was already pointed out in the beginning of this section that the above formulae (12), (13), (14), (15) and (17) remain valid for incomplete polarization of the target, the vector  $s \equiv s_i$  being recognized as the polarization vector of the density matrix  $\rho_i$  for the initial nucleon. The density

matrix for the final nucleon  $\rho_f \equiv \frac{1}{2}(\hat{q} + m_f)(1 - \gamma_5 \hat{s}_f)$  is given by

$$\rho_f = \frac{(\hat{q} + m_f) \hat{M}(i\gamma_5) \rho_i \gamma_0 (i\gamma_5)^\dagger \hat{M}^\dagger \gamma_0 (\hat{q} + m_f)}{\text{Sp} [(\hat{q} + m_f) \hat{M}(i\gamma_5) \rho_i \gamma_0 (i\gamma_5)^\dagger \hat{M}^\dagger \gamma_0]}. \quad (24)$$

The expression for the polarization vector  $s_f$  takes the form

$$s_f^\mu = \frac{1}{2m_f} \frac{M^T F^\mu M^*}{M^T G M^*}, \quad (25)$$

where  $G$  is given by eqs. (13), (14), (15) and the array of matrices  $F^\mu$  can be calculated as

$$F^\mu \equiv \text{Sp} \left[ (\hat{q} + m_f) \begin{Bmatrix} \hat{1} \\ 2\hat{k}_R \\ 2\hat{k}_I \\ [\hat{k}_R, \hat{k}_I] \end{Bmatrix} (\hat{p} - m_i) \frac{1 + \gamma_5 \hat{s}_i}{2} \gamma_0 \begin{Bmatrix} \hat{1} \\ 2\hat{k}_R \\ 2\hat{k}_I \\ [\hat{k}_R, \hat{k}_I] \end{Bmatrix}^\dagger \gamma_0 (\hat{q} + m_f) \gamma_5 \gamma^\mu \right]. \quad (26)$$

The calculation with the use of the standard High Energy Physics package of computer algebra [42] is straightforward, the result being too cumbersome to be displayed here.

Values of  $s_f$  and  $A_{(\mathbf{x}, \mathbf{y})}(\varphi_{\mathbf{z}})$  are defined over 4-dimensional phase space of the considered reaction. This makes it difficult to display such quantities visually. Below, we consider asymmetries which are integrated as over “orange lobules” of  $\varphi_{\mathbf{z}}$  bins,  $\mathbf{z}$  being a selected momentum, as well as over allowed range of the rest momenta. This averaging suppresses the polarization effect. The suppression depends upon the kinematical symmetry of the considered amplitude: the more symmetry is displayed by the amplitude, the less value of the averaged asymmetry  $A_{(\mathbf{x}, \mathbf{y})}(\varphi_{\mathbf{z}})$  is obtained. It was shown in the paper [39] that form factors  $S, V^R, V^I, T$  of isoscalar amplitudes  $A, B, C, D$  had definite properties under permutation of nucleons  $p \leftrightarrow -q$  due to charge-conjugation symmetry, the properties of  $D$ -amplitude form factors being opposite to the ones of the corresponding form factors of the rest isoscalar amplitudes. Another symmetry of particle momenta, that eliminates the kinematical degrees of freedom, is related to Bose statistics of identical pions in  $\{++n\}$  and  $\{00n\}$  channels. The expressions for channel amplitudes given by eqs. 4 show that the asymmetries for the above two channels are more suffering from the discussed degeneracies while channels  $\{\pm 0 p\}$ , being free from the ones, can display less suppression under averaging. It is obvious that the rare events in the reaction represent the only reason for considering the integral quantities.

## 4 Simulation of Data and Results

It is found necessary to study asymmetries of cross sections with respect to various planes in momentum space. The complicated form of the phenomenological amplitude makes it impossible

to perform an analytic investigation of the polarization term of the matrix element (17). In the absence of real experimental measurements, we perform theoretical simulations. Prior to discussion of their details given below, let us briefly consider the geometry of the existing CHAOS device which is capable to provide the necessary measurements (for more details see [33, 43, 44]).

The cylindrical dipole magnet, producing the vertical magnetic field, is the largest part of the CHAOS spectrometer. A polarized target is exposed to the horizontal pion beam. The target is inserted through the 120 mm calibre hole along magnet's symmetry axis. So the target is placed at the center of the cylindrical space between the magnet poles, the pole diameter being 950 mm. Four cylindrical chambers are surrounding the target: the most inner WC1 and WC2 are fast multi-wire proportional chambers, WC3 and WC4 are the drift chambers.

The ring of gain stabilized counter telescopes constitutes the outside layer of detectors. These counters determine the vertical acceptance of  $\pm 7^\circ$ . In the horizontal plane (CHAOS plane), there are deadened regions of WC3 and WC4 in narrow angles ( $\approx 36^\circ$  in total) where the beam enters and exits the device. This causes a difficulty for tracking and particle identification for some events. The angle and momentum value of an outgoing charged particle hitting only WC1 and WC2 and missing WC3 and/or WC4 are correlated because of the magnetic field present. We neglect this effect and simply set the horizontal acceptance to  $360^\circ$ . Apart from geometrical cuts, no extra factors such as efficiencies of registration, etc. are involved into our simulations for simplicity.

Though some structures of polarized cross sections, like that of eqs. (19), (22), have no explicit dependence upon the relative orientation of the nucleon-spin vector  $s$  and the beam  $k_1$ , we consider two basic variants with respect to this orientation in the laboratory system. This is natural for the design of experimental devices and this is convenient for data simulations as well. So  $\mathbf{s}$  is chosen to be orthogonal to the beam  $\mathbf{k}_1$  and to the CHAOS plane in the first variant ( $\mathbf{s} \perp \mathbf{k}_1$ ) and  $\mathbf{s}$  is chosen to be parallel to the beam  $\mathbf{k}_1$  in the second variant ( $\mathbf{s} \parallel \mathbf{k}_1$ ).

The Monte-Carlo events for the reaction channel  $\pi^- p^\uparrow \rightarrow \pi^- \pi^+ n$  are generated at the beam momentum set to  $P_{\text{Lab}} = 360 \text{ MeV}/c$ . Few control runs are performed also for the rest channels at the same energy. We consider the azimuth angle in the orthogonal to  $(\mathbf{x}, \mathbf{y})$  plane through the vector  $\mathbf{y}$ . The angle is counted out from the direction  $\mathbf{y}$ . The bins for this angle are filled with the selection of events **a)** without geometrical restrictions and **b)** with restrictions of CHAOS geometry (CHAOS is hit by 46 307 events from the requested amount of 2 000 000).

The list of examined asymmetries  $A_{(\mathbf{x}, \mathbf{y})}(\varphi_{\mathbf{z}})$  can be obtained from the headings of the figures 1–4. By obvious geometrical reasons the list for the variant ( $\mathbf{s} \parallel \mathbf{k}_1$ ) is truncated. The list is far from being complete combinatorically. Nevertheless, it is sufficient to display the role of distinct

Ampl.	$a_0^{I=0}$	$a_0^{I=2}$	$a_1^{I=1}$	$(\mathbf{s} \perp \mathbf{k}_1)$ $4\pi$	$(\mathbf{s} \perp \mathbf{k}_1)$ CHAOS	$(\mathbf{s} \parallel \mathbf{k}_1)$ $4\pi$
solw6	0.264	-0.008	0.032	$0.89(4)_{(\mathbf{s}, \mathbf{q})}(\mathbf{k}_1)$	$0.91(7)_{(\mathbf{s}, \mathbf{q})}(\mathbf{k}_1)$	$0.259(4)_{(\mathbf{q}, \mathbf{k}_I)}(\mathbf{k}_R)$
sol05	0.193	0.074	-0.014	$0.251(9)_{(\mathbf{s}, \mathbf{q})}(\mathbf{k}_R)$	$0.5(5)_{(\mathbf{s}, \mathbf{q})}(\mathbf{k}_R)$	$0.203(4)_{(\mathbf{q}, \mathbf{k}_I)}(\mathbf{k}_R)$
sol06	0.189	-0.059	0.054	$-0.38(4)_{(\mathbf{s}, \mathbf{k}_1)}(\mathbf{k}_R)$	$-0.40(6)_{(\mathbf{s}, \mathbf{k}_1)}(\mathbf{k}_R)$	$0.089(6)_{(\mathbf{q}, \mathbf{k}_I)}(\mathbf{k}_R)$
sol04	0.175	0.048	-0.084	$[-0.23(3)_{(\mathbf{s}, \mathbf{k}_1)}(\mathbf{q})]$	$[0.22(2)_{(\mathbf{s}, \mathbf{k}_I)}(\mathbf{k}_R)]$	$0.093(3)_{(\mathbf{s}, \mathbf{q})}(\mathbf{k}_I)$
sol10	0.172	-0.043	0.050	$-0.41(3)_{(\mathbf{s}, \mathbf{k}_1)}(\mathbf{q})$	$0.39(4)_{(\mathbf{s}, \mathbf{q})}(\mathbf{k}_1)$	$0.133(3)_{(\mathbf{q}, \mathbf{k}_I)}(\mathbf{k}_R)$
sol07	0.156	0.002	0.043	$0.070(3)_{(\mathbf{s}, \mathbf{q})}(\mathbf{k}_2)$	$0.12(4)_{(\mathbf{s}, \mathbf{k}_I)}(\mathbf{k}_R)$	$0.155(3)_{(\mathbf{q}, \mathbf{k}_I)}(\mathbf{k}_R)$
sol02	0.105	0.036	-0.027	$[-0.29(4)_{(\mathbf{s}, \mathbf{k}_1)}(\mathbf{q})]$	$[0.25(4)_{(\mathbf{s}, \mathbf{q})}(\mathbf{k}_1)]$	$0.273(4)_{(\mathbf{q}, \mathbf{k}_I)}(\mathbf{k}_R)$
sol09	0.077	-0.006	0.036	$-0.52(5)_{(\mathbf{s}, \mathbf{q})}(\mathbf{k}_1)$	$0.55(6)_{(\mathbf{s}, \mathbf{k}_1)}(\mathbf{q})$	$0.284(4)_{(\mathbf{q}, \mathbf{k}_I)}(\mathbf{k}_R)$
sol01	0.069	0.030	0.023	$-0.58(4)_{(\mathbf{s}, \mathbf{q})}(\mathbf{k}_1)$	$0.61(6)_{(\mathbf{s}, \mathbf{k}_1)}(\mathbf{q})$	$0.290(4)_{(\mathbf{q}, \mathbf{k}_I)}(\mathbf{k}_R)$
sol03	0.069	-0.057	0.045	$-0.29(3)_{(\mathbf{s}, \mathbf{k}_1)}(\mathbf{q})$	$0.25(4)_{(\mathbf{s}, \mathbf{q})}(\mathbf{k}_1)$	$0.265(8)_{(\mathbf{s}, \mathbf{k}_I)}(\mathbf{k}_2)$
sol11	0.067	-0.077	0.047	$0.48(3)_{(\mathbf{s}, \mathbf{k}_1)}(\mathbf{q})$	$0.52(5)_{(\mathbf{s}, \mathbf{k}_1)}(\mathbf{q})$	$0.224(7)_{(\mathbf{q}, \mathbf{k}_I)}(\mathbf{k}_R)$
sol12	0.011	-0.008	-0.030	$-0.281(3)_{(\mathbf{s}, \mathbf{q})}(\mathbf{k}_3)$	$0.42(3)_{(\mathbf{s}, \mathbf{k}_I)}(\mathbf{k}_R)$	$0.381(4)_{(\mathbf{q}, \mathbf{k}_I)}(\mathbf{k}_R)$

Table 1: The largest asymmetries for  $\pi^- p \rightarrow \pi^- \pi^+ n$  channel at  $P_{\text{Lab}} = 360$  MeV/c. The last-digit errors are given in brackets. The square brackets indicate the results for asymmetries developed under vanishing cross sections.

structures and to demonstrate tight relations between quantities like  $A_{(\mathbf{s}, \mathbf{k}_1)}(\varphi_{\mathbf{q}})$  and  $A_{(\mathbf{s}, \mathbf{q})}(\varphi_{\mathbf{k}_1})$ .

Twelve amplitudes for  $\pi N \rightarrow \pi\pi N$  reactions, all of which but one being found as solutions of analysis [9] of unpolarized data, are used as the theoretical input. These solutions are practically equivalent by the  $\chi^2$  criterion. Such properties of solutions like  $\chi^2$ , errors of parameters, etc. are irrelevant for simulations. We show only specific values of  $\pi\pi$ -scattering lengths in Table 1. The ordering of solutions in this Table is performed according to the value of  $a_0^{I=0}$ . This reflects the role of OPE in the given amplitude: it is negligible for amplitudes from the bottom of Table 1. The discussed amplitudes can be split into two classes: the *physical* amplitudes, which support the sequence of signs  $\{ "+", "-", "+" \}$  for scattering lengths  $a_0^{I=0}, a_0^{I=2}, a_1^{I=1}$ , and the rest amplitudes which we call *unphysical*.

The amount of obtained data is too large to be displayed here. The following Table 1 collects the largest values of integral asymmetries found for discussed amplitudes. Sometimes, a lower value is given if it is characterized by better accuracy. The given errors are only the statistical ones. This can help to estimate what number of experimental events is sufficient to detect the asymmetry in question.

All data for asymmetries were also represented in the graphical form. Only few of them are shown in figs. 1–6 for illustrative purpose. For example, a comparison of fig. 1 with fig. 2 and fig. 3 with fig. 4 helps to make conclusions on the role of initial-spin orientation and on different

properties of CHAOS selections. Comparing figs. 1, 2 with figs. 3, 4, one finds quite individual polarization phenomena for different solutions.

The collection of pictures is found to have a striking property: all solutions, being indistinguishable by  $\chi^2$  in the course of analysis [9], appear to be different.

The examination of pictures shows also that the asymmetries  $A_{(s,q)}(\varphi_{\mathbf{k}_1})$ ,  $A_{(s,q)}(\varphi_{\mathbf{k}_R})$ ,  $A_{(s,\mathbf{k}_1)}(\varphi_{\mathbf{q}})$  are characteristic of the OPE mechanism. These asymmetries become smaller and other asymmetries start to appear when one is going from solutions from the top of Table 1 to solutions from the bottom, i.e. “switching off” the OPE contribution.

Another important feature of the obtained data is related to unresolved ambiguity between the physical and unphysical solutions. It is found that the latter develop smaller asymmetries. Generally, the asymmetries for unphysical solutions are more difficult to detect, since they are peaking in narrow angles characterized by low cross sections. In contrast, when asymmetries for physical amplitudes reach the maximal values, the curves are gently sloping. The found absolute maximum  $A \sim 1$  corresponds usually to directions with small cross sections (see distributions at  $\varphi = 40^\circ$  given in fig. 5; the corresponding asymmetry  $A_{(s,q)}(\varphi_{\mathbf{k}_1})$  can be found in fig. 1). There are enough statistics for the nearby angles to detect the relatively high value of such asymmetry, for example, at  $\varphi \sim 20^\circ$ , see fig. 5.

When putting aside the last amplitudes from Table 1 and splitting the rest into physical and unphysical groups, a regular behaviour of pictures with the parameter  $a_0^{I=2}$  can be found in both groups. This is demonstrated by fig. 6, where the asymmetries for physical amplitudes sol06, sol03, sol10 and solw6 are shown at  $(\mathbf{s} \perp \mathbf{k}_1)$ . The almost smooth transformation of one picture into another is clearly seen for asymmetries, which are relevant to OPE. This regularity and the absence of the same regularity for  $a_0^{I=0}$  variation can be interpreted as an indirect evidence in favour of smaller perturbations by isobar contributions to isospin  $I = 2$  amplitude. However, poor asymmetries from OPE and rich the rest ones obtained for  $\pi^+ p^\uparrow \rightarrow \pi^+ \pi^+ n$  channel do not support this.

These conclusions are valid for measurements with  $(\mathbf{s} \perp \mathbf{k}_1)$  in devices with  $4\pi$ -steradian geometry and in the CHAOS device as well. Moreover, the CHAOS geometry selects events displaying larger asymmetries, though at the price of lower statistics.

The asymmetries for the setup  $(\mathbf{s} \parallel \mathbf{k}_1)$  are rich and informative for the  $4\pi$ -steradian geometry of a hypothetical device. Here, the asymmetries  $A_{(q,\mathbf{k}_1)}(\varphi_{\mathbf{z}})$ ,  $A_{(q,\mathbf{k}_I)}(\varphi_{\mathbf{z}})$ ,  $A_{(k_2,k_3)}(\varphi_{\mathbf{z}})$  ( $\mathbf{z} = \mathbf{k}_1, \mathbf{k}_2, \mathbf{k}_3, \mathbf{k}_R, \mathbf{k}_I, \mathbf{q}$ ), all of which are almost flat for  $(\mathbf{s} \perp \mathbf{k}_1)$  setup, are looking much more vivid (cf. figs. 1 and 2). According to criteria of sect. 3, the “switching off” effect of  $(\mathbf{s} \cdot \mathbf{k}_R) \sim -(\mathbf{s} \cdot \mathbf{k}_1) = 0$  must be solely due to non-OPE mechanisms in the test amplitudes. These are indeed present in

all discussed solutions.

When projected to CHAOS, all examined asymmetries for  $(\mathbf{s}||\mathbf{k}_1)$  appear to be consistent with zero. This is not so surprising, since, for the  $(\mathbf{s}||\mathbf{k}_1)$  setup, practically all interesting events happen in the plane which is orthogonal to the beam  $\mathbf{k}_1$ . The most part of such events avoids CHAOS chambers. Though the cross sections themselves are found to be sensitive to the tested amplitudes in the forward and backward cones, it is difficult to evaluate the importance of such data. One can recall that the above critical plane is entirely accepted by the wire-chamber space of the design for the AMPIR spectrometer [41]. This remarkable complementarity of CHAOS and AMPIR devices makes a promise for exhaustive investigations of polarization effects in  $\pi N \rightarrow \pi\pi N$  reactions at low energies.

We finish the discussion of results by reminding that there are simplifications in the procedure. The incomplete polarization in the real experiment can decrease the absolute values of the shown asymmetries by few percent. The real-device efficiency and the reduced experimental statistics enlarge errors. The number of generated events in simulations ( $\sim 4 \times 10^4$  hitting CHAOS) represents the limit ever attainable experimentally. Provided no confident result is obtained, the problem of polarization phenomena below isobar threshold  $P_{\text{Lab}} < 500$  MeV/c would be closed. The rich picture of effects displayed by almost every amplitude at  $P_{\text{Lab}} = 360$  MeV/c is far above cautious expectations. The magnitude of statistical errors given in Table 1 demonstrates that the number of experimental events which is necessary to detect the discussed phenomena and discriminate between competing contributions, can be decreased by an order of magnitude. It must be noted that reaction channel  $\pi^- p^\uparrow \rightarrow \pi^- \pi^+ n$  is not the best one in respect to integral asymmetries examined in this section. Simulations with some selected amplitudes show the following order of preference:  $\pi^+ p^\uparrow \rightarrow \pi^+ \pi^0 p$ ,  $\pi^- p^\uparrow \rightarrow \pi^- \pi^0 p$ ,  $\pi^- p^\uparrow \rightarrow \pi^- \pi^+ n$ ,  $\pi^+ p^\uparrow \rightarrow \pi^+ \pi^+ n$ ,  $\pi^- p^\uparrow \rightarrow \pi^0 \pi^0 n$ . This means that the neutral channel requires full-kinematics measurements for detecting asymmetries in distinct regions of the entire phase space.

## 5 Conclusions

The main achievement of the present paper is the demonstration of striking efficiency of the polarization measurements for  $\pi N \rightarrow \pi\pi N$  reactions in the very close to threshold energy region. Such measurements are feasible with the use of CHAOS spectrometer right now. This is shown in the framework of the standard formalism adjusted to the canonical form of the  $\pi N \rightarrow \pi\pi N$  amplitude [38, 40].

The motivation for such experiments follows from disappointing difficulties encountered within frameworks of all known methods for the analysis of low-energy  $\pi N \rightarrow \pi\pi N$  data. The deep reason of difficulties in the interpretation of the  $\pi N \rightarrow \pi\pi N$  results is related to the very nature of the unpolarized data which cannot help to discriminate between the  $t$ -channel mechanism of OPE and isobar exchanges.

The competition between OPE and the rest mechanisms of  $\pi N \rightarrow \pi\pi N$  reaction, preventing from accurate determination of  $\pi\pi$  interaction with the help of unpolarized data, at the same time gives rise to extremely rich polarization effects within half-width isobar region.

The effects are found to be sensitive as to the OPE parameters in question as well as to details of isobar interactions. All equivalent solutions of the paper [9] appear to be different in the asymmetry picture. Therefore, any project of determination of parameters of  $\pi\pi$  interaction with the help of  $\pi N \rightarrow \pi\pi N$  data must assume the polarization measurements. The yield for the decisive  $\pi N \rightarrow \pi\pi N$  analysis must combine both unpolarized data and polarization information.

The application of results of the present paper is straightforward within the method **3** mentioned in Introduction. It is simple to find that all asymmetries vanish in the extrapolation points specific to methods **1** and **2**. This can help to estimate a part of the theoretical error characteristic of a method. Indeed, provided the data of polarized-target experiments are collected separately from right and left semi-spheres with respect to  $(\mathbf{s}, \mathbf{k}_1)$ ,  $(\mathbf{s}, \mathbf{q})$  or  $(\mathbf{q}, \mathbf{k}_1)$  planes, the estimate of error is obtained by the independent extrapolations.

## 6 Acknowledgments

AAB and SGS thank Russian Federation for Basic Research for support in terms of grant N 95-02-05574a. We are grateful to G.A. Feofilov and D. Počanić for remarks and to members of CHAOS collaboration P. Amaudruz, F. Bonutti, J. Brack, P. Camerini, E. Fragiaco, N. Grion, G. Hofman, R.R. Johnson, S. McFarland, M. Kermani, R. Rui, M. Sevier, G.R. Smith, R. Tacik for various help and discussions.

## References

- [1] J. Gasser and H. Leutwyler. Phys. Lett. **125B** (1982) 312; Phys. Lett. **125B** (1982) 325.
- [2] J. Gasser and H. Leutwyler. Ann. Phys. (NY) **158** (1984) 142; Nucl. Phys. **B250** (1985) 465, 517, 539.
- [3] S. Weinberg. Phys. Rev. Lett. **17** (1966) 616.
- [4] S. Weinberg. Phys. Rev. **166** (1968) 1568.
- [5] S. Weinberg. Physica **96A** (1979) 327
- [6] J. Stern, H. Sazdjian and N.H. Fuchs. Phys. Rev. **D47** (1993) 3814.
- [7] D. Počanić. Summary of  $\pi$ - $\pi$  Scattering Experiments, *in* A.M. Bernstein and B.R. Holstein (eds.), Chiral Dynamics: Theory and Experiment, Proceedings of the Workshop held at MIT, Cambridge, MA, USA, 25–29 July 1994, Lecture Notes in Physics, LNP 452 (Springer–Verlag, Berlin and Heidelberg, 1995), p. 95.
- [8] D. Počanić. *Low Energy Experiments on  $\pi$ - $\pi$  Scattering*, preprint UVA-INPP-98-01, Sep. 1997. 16pp. *Talk given at Workshop on Chiral Dynamics: Theory and Experiment (ChPT 97), Mainz, Germany, 1-5 Sep 1997;* preprint hep-ph/9801366, 16pp. 1998.
- [9] A.A. Bolokhov, M.V. Polyakov and S.G. Sherman. EPJ A **1** (1998) 3, 317–336.
- [10] D. Počanić and E. Frlež. Nucl. Phys. **A629** (1998) 201–204; hep-ph/9706553.
- [11] M.G. Olsson. Rigorous pion–pion scattering lengths from threshold  $\pi N \rightarrow \pi\pi N$  data. Preprint MADPH-97-988, March 1997, 13p.; hep-ph/9703247.
- [12] O.O. Patarakin. “A Measurement of the  $\pi^\pm p \rightarrow \pi^+ \pi^\pm n$  Reactions Near Threshold.” *in* Ulf–G. Meissner, M. Sevier, A. Badertscher, et al. *Working Group on  $\pi\pi$  and  $\pi N$  Interactions. Summary.* KFA-IKP-TH-1997-21, Nov 1997. p10; *Summary of the working group on  $\pi\pi$  and  $\pi N$  interactions given at Workshop on Chiral Dynamics: Theory and Experiment (ChPT 97), Mainz, Germany, 1-5 Sep 1997.;* hep-ph/9711361.
- [13] M.E. Sevier. “Determination of the  $\pi^\pm p \rightarrow \pi^\pm \pi^\pm n$  Cross–Sections Near Threshold.” *in* Ulf–G. Meissner, M. Sevier, A. Badertscher, et al. *Working Group on  $\pi\pi$  and  $\pi N$  Interactions.*



- Summary.* KFA-IKP-TH-1997-21, Nov 1997. p11; *Summary of the working group on  $\pi\pi$  and  $\pi N$  interactions given at Workshop on Chiral Dynamics: Theory and Experiment (ChPT 97), Mainz, Germany, 1-5 Sep 1997.*; hep-ph/9711361.
- [14] M.G. Olsson and L. Turner. Phys. Rev. Lett. **20** (1968) 1127; Phys. Rev. **181** (1969) 2141; Phys. Rev. **D6** (1972) 3522.
  - [15] C.J. Goebel. Phys. Rev. Lett. **1**, (1958) 337; G.F. Chew and F.E. Low. Phys. Rev. **113** (1959) 1640.
  - [16] E. Oset and M.J. Vicente–Vacas. Nucl. Phys. A **446** (1985) 584.
  - [17] G. Kernel, D. Korbar, et al. Phys. Lett., **B225** (1989) 198-202.
  - [18] G. Kernel, D. Korbar, et al. Phys. Lett., **B216** (1989) 244-248.
  - [19] G. Kernel, D. Korbar, et al. Z. Phys. **C48** (1990) 201.
  - [20] G. Kernel, et al. OMICRON. Z. Phys. **C51** (1991) 377.
  - [21] M.E. Sevior, A. Ambardar, et al. Phys. Rev. Lett. **66** (1991) 2569-2572.
  - [22] J. Lowe, B. Bassalleck, et al. Phys. Rev. **C44** (1991) 956-965.
  - [23] D. Počanić, E. Frlež, K.A. Assamagan, et al. Phys. Rev. Lett. **72** (1994) 1156.
  - [24] V. Bernard, N. Kaiser and Ulf-G. Meißner. Phys. Lett. **B332** (1994) 415; **B338** (1994) 520;
  - [25] M.G. Olsson, Ulf-G. Meißner, N. Kaiser and V. Bernard. “On the interpretation of the  $\pi N \rightarrow \pi\pi N$  data near threshold”.  $\pi N$  Newsletter **10**, 201 (1995); Preprint CRN 95-13, MADPH-95-866, TK 95 07 (1995).
  - [26] V. Bernard, N. Kaiser and Ulf-G. Meißner. Nucl. Phys. **B457** (1995) 147.
  - [27] Ulf-G. Meißner. *The Reaction  $\pi N \rightarrow \pi\pi N$  at Threshold.* Talk given at 7th International Conference on the Structure of Baryons, Santa Fe, NM, 3–7 Oct. 1995. Preprint TK 95 29 (1995) 4p.; hep-ph/9510390.
  - [28] V. Bernard, N. Kaiser and Ulf-G. Meißner. *The Reaction  $\pi N \rightarrow \pi\pi N$  above Threshold in Chiral Perturbation Theory.* Nucl. Phys. **A619** (1997) 261-284; Preprint KFA-IKP(TH)-1997-05, Mar. 1997, 29p.; hep-ph/9703218.

- [29] V. Bernard, N. Kaiser and Ulf-G. Meißner. *The Reaction  $\pi N \rightarrow \pi\pi N$  in HBCHPT.* in J. Bijnens (Nordita), U.G. Meissner (Bonn U.). *Workshop on the Standard Model at Low Energies: Miniproceedings*, Contributed to International Workshop on The Standard Model at Low Energies, Trento, Italy, 29 Apr - 10 May 1996. ECT-96-010, Apr 1996, p12; hep-ph/9606301.
- [30] A.A. Bolokhov and S.G. Sherman. *Phenomenological  $\pi N \rightarrow \pi\pi N$  Amplitude and the Modelling of the Olsson–Turner and Chew–Low approaches.* Submitted to EPJ.
- [31] G.A. Leikin. Uspekhi., **102**, 387–430, 1970.
- [32] B.R. Martin, D. Morgan and G. Shaw. Pion–Pion Interactions in Particle Physics. Academic Press, NY, 1976.
- [33] G.R. Smith, et al. Nucl. Instr. and Meth. **A362** (1995) 349.
- [34] A.de Lesquen, et al. Phys. Rev. **D32** (1985) 21.
- [35] G. Grayer, et al. Nucl. Phys. **B75** (1974) 189.
- [36] M. Svec. Phys. Rev. **D46** (1992) 949.
- [37] H. Becker, et al. Nucl. Phys. **B151** (1979) 46.
- [38] A.A. Bolokhov, V.V. Vereshchagin and S.G. Sherman. Yad. Fiz., 47, 491–493, 1988.
- [39] A.A. Bolokhov, V.V. Vereshchagin and M.V. Polyakov. Yad. Fiz., 48, 811–813, 1988.
- [40] A.A. Bolokhov, V.V. Vereshchagin and S.G. Sherman. Nucl. Phys. **A530** (1991) 660.
- [41] A.B. Kurepin, V.A. Krasnov, Yu.K. Gavrilov, et al. *Spectrometer AMPIR for Investigation of Rare and Multiparticle Processes.* Inst. for Nuclear Research, Russian Academy of Sciences. Preprint INR-769/92. Moscow, 1992. 15 pp.
- [42] A.C. Hern. REDUCE User’s Manual. Rand Corp., Santa Monica. 1985.
- [43] F. Bonutti et al., Nucl. Instr. and Meth. **A337** (1993) 165.
- [44] F. Bonutti et al., Nucl. Instr. and Meth. **A350** (1994) 136.

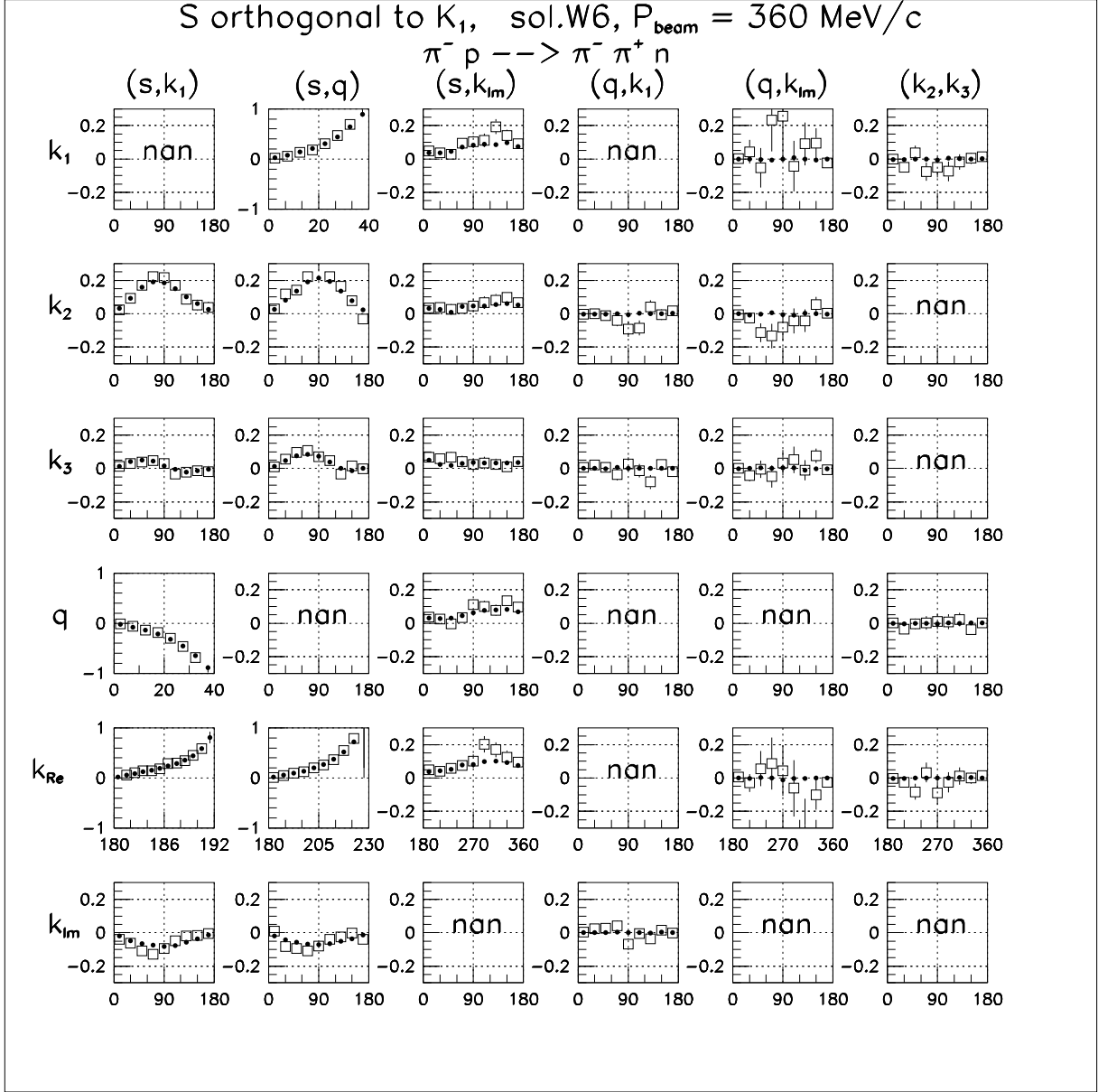


Figure 1: Asymmetries for the amplitude solw6 at  $(\mathbf{s} \perp \mathbf{k}_1)$  in the  $4\pi$ -steradian geometry device (full dots) and in CHAOS (open squares).

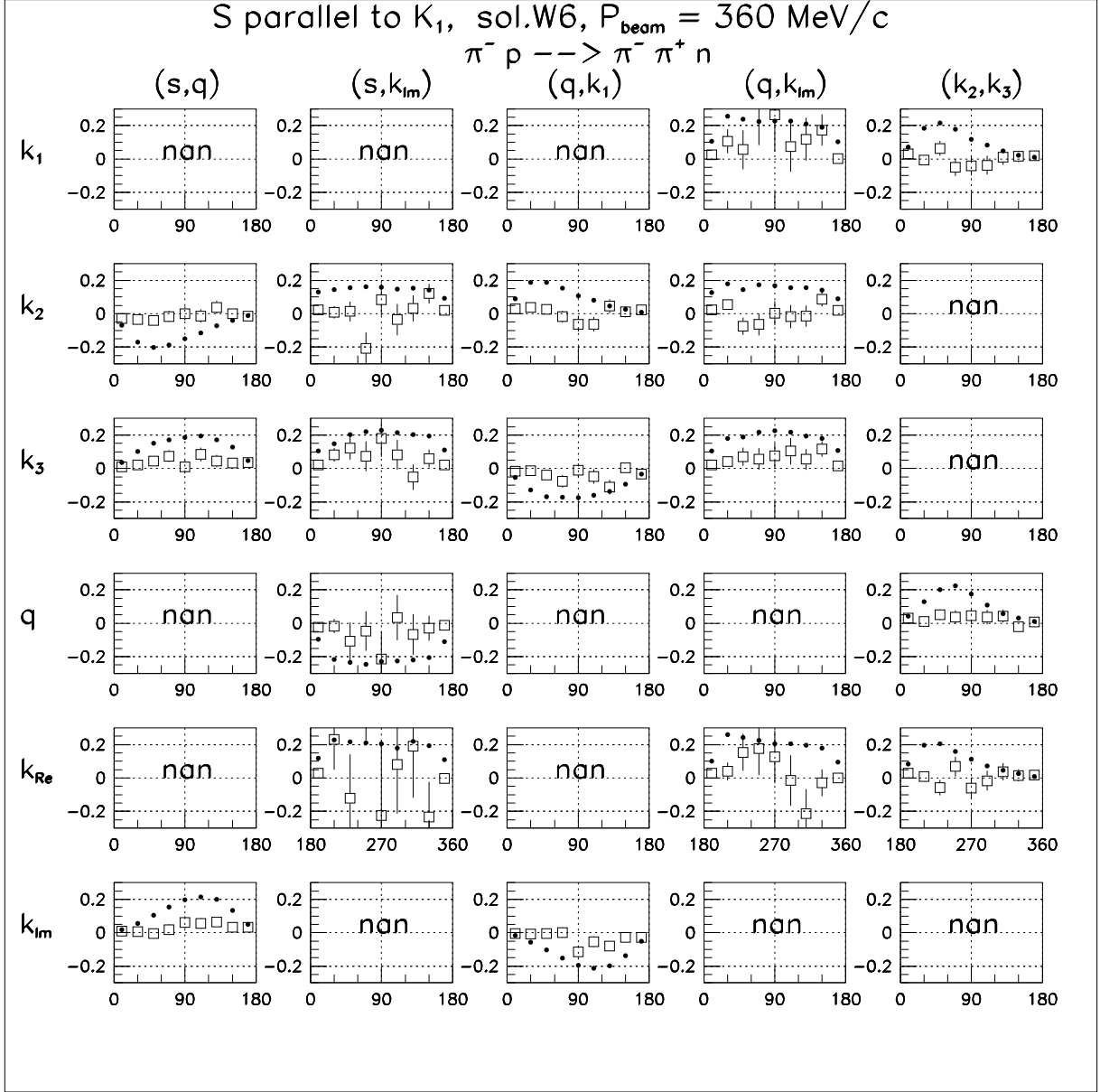


Figure 2: Asymmetries for the amplitude solw6 at  $(s||\mathbf{k}_1)$  in the  $4\pi$ -steradian geometry device (full dots) and in CHAOS (open squares).

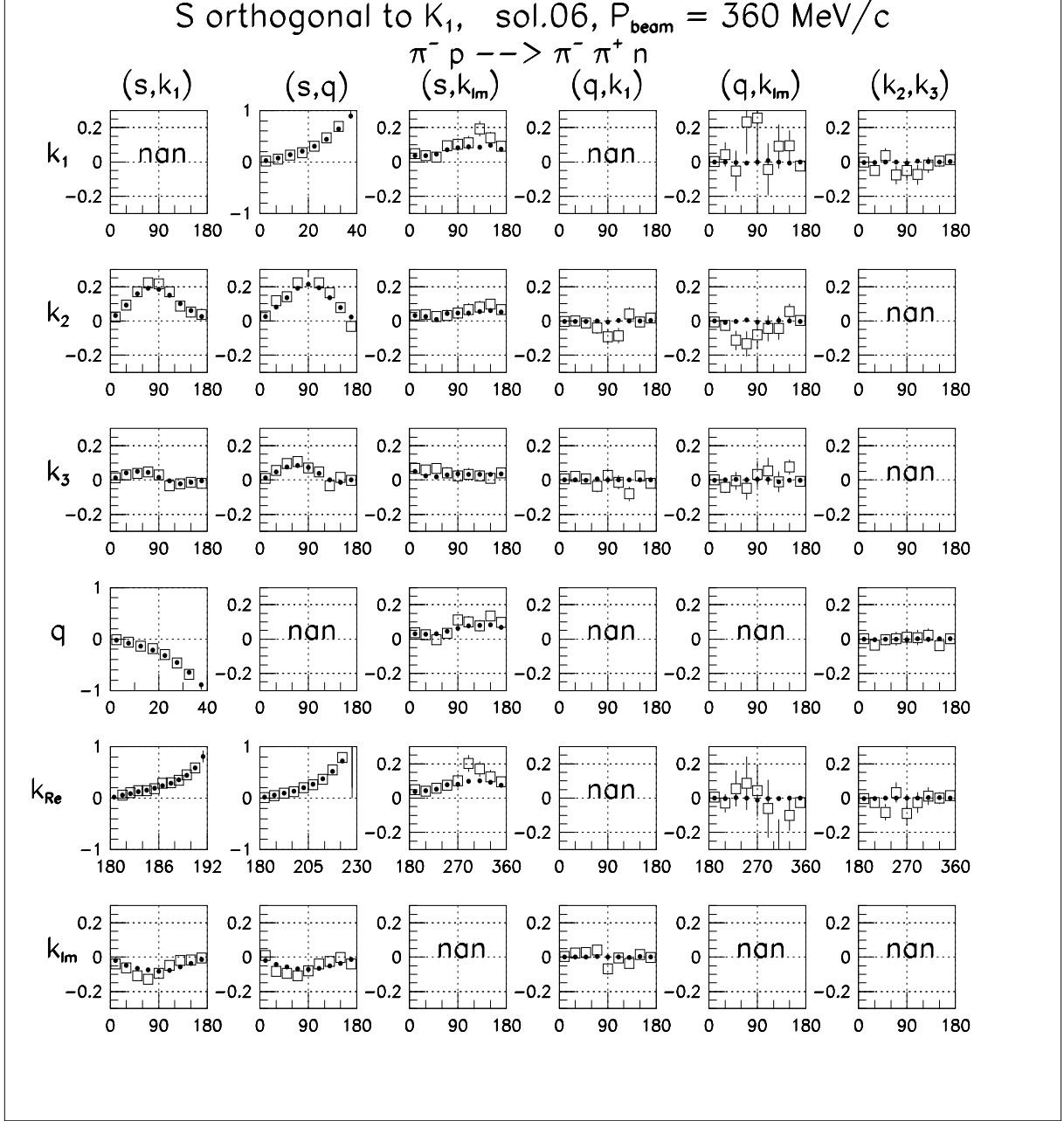


Figure 3: Asymmetries for the amplitude sol06 at  $(\mathbf{s} \perp \mathbf{k}_1)$  in the  $4\pi$ -steradian geometry device (full dots) and in CHAOS (open squares).

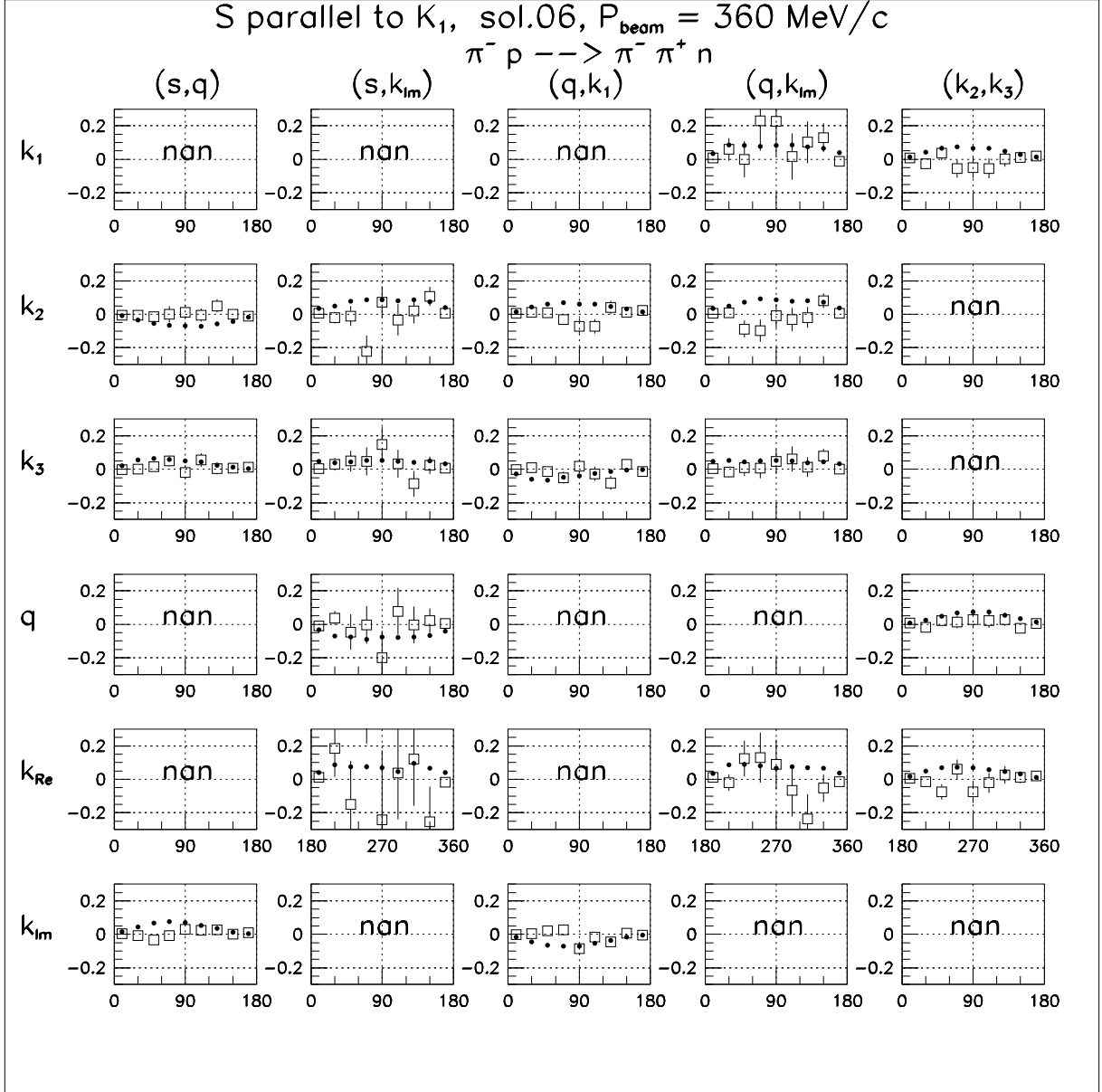


Figure 4: Asymmetries for the amplitude sol06 at  $(s||\mathbf{k}_1)$  in the  $4\pi$ -steradian geometry device (full dots) and in CHAOS (open squares).

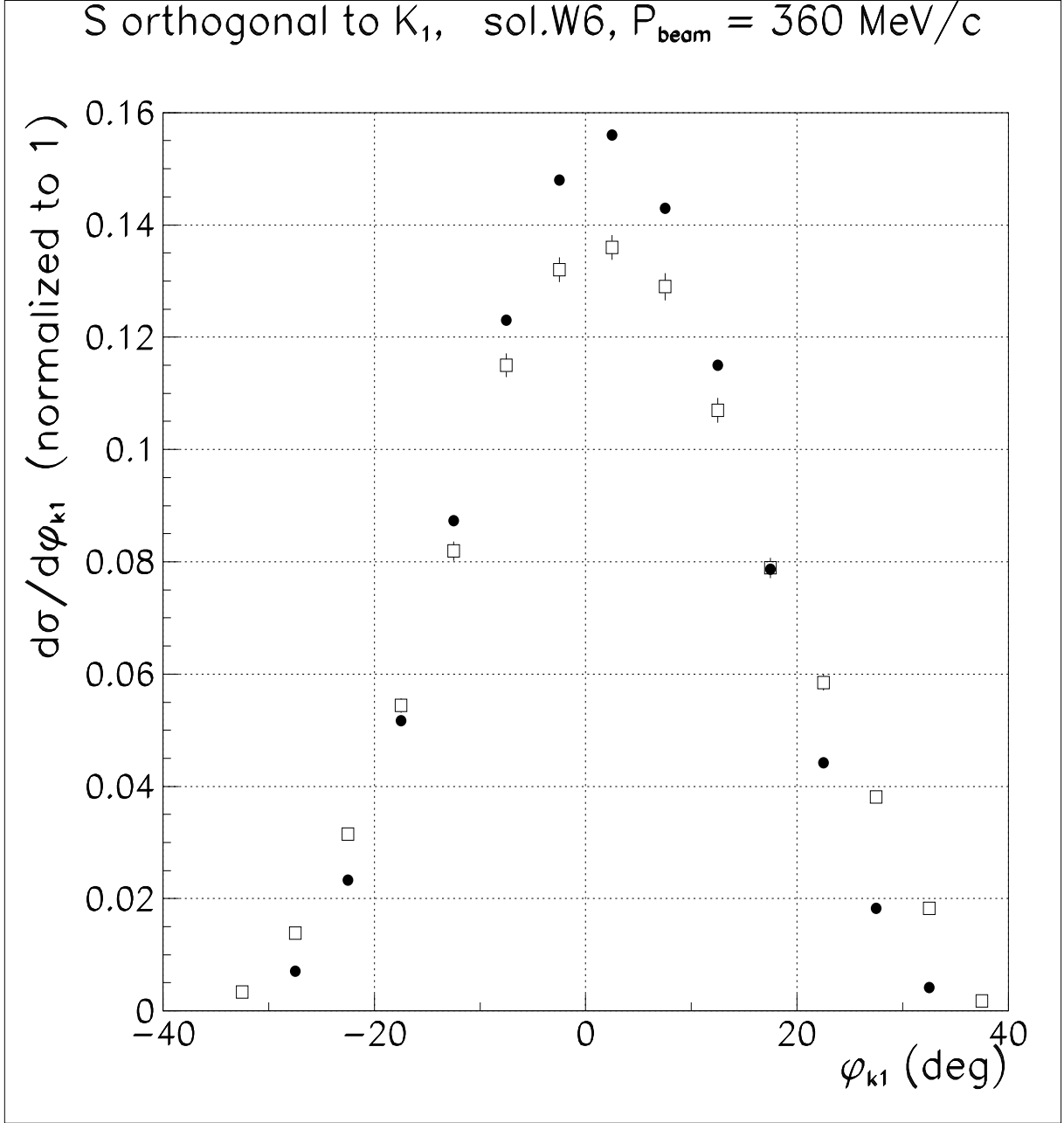


Figure 5: Distributions in the azimuth angle of  $\mathbf{k}_1$  projected to the the plane through  $\mathbf{q}$  and orthogonal to the plane  $(\mathbf{s}, \mathbf{q})$  for the amplitude solw6 at  $(\mathbf{s} \perp \mathbf{k}_1)$  in the  $4\pi$ -steradian geometry device (full dots) and in CHAOS (open squares).

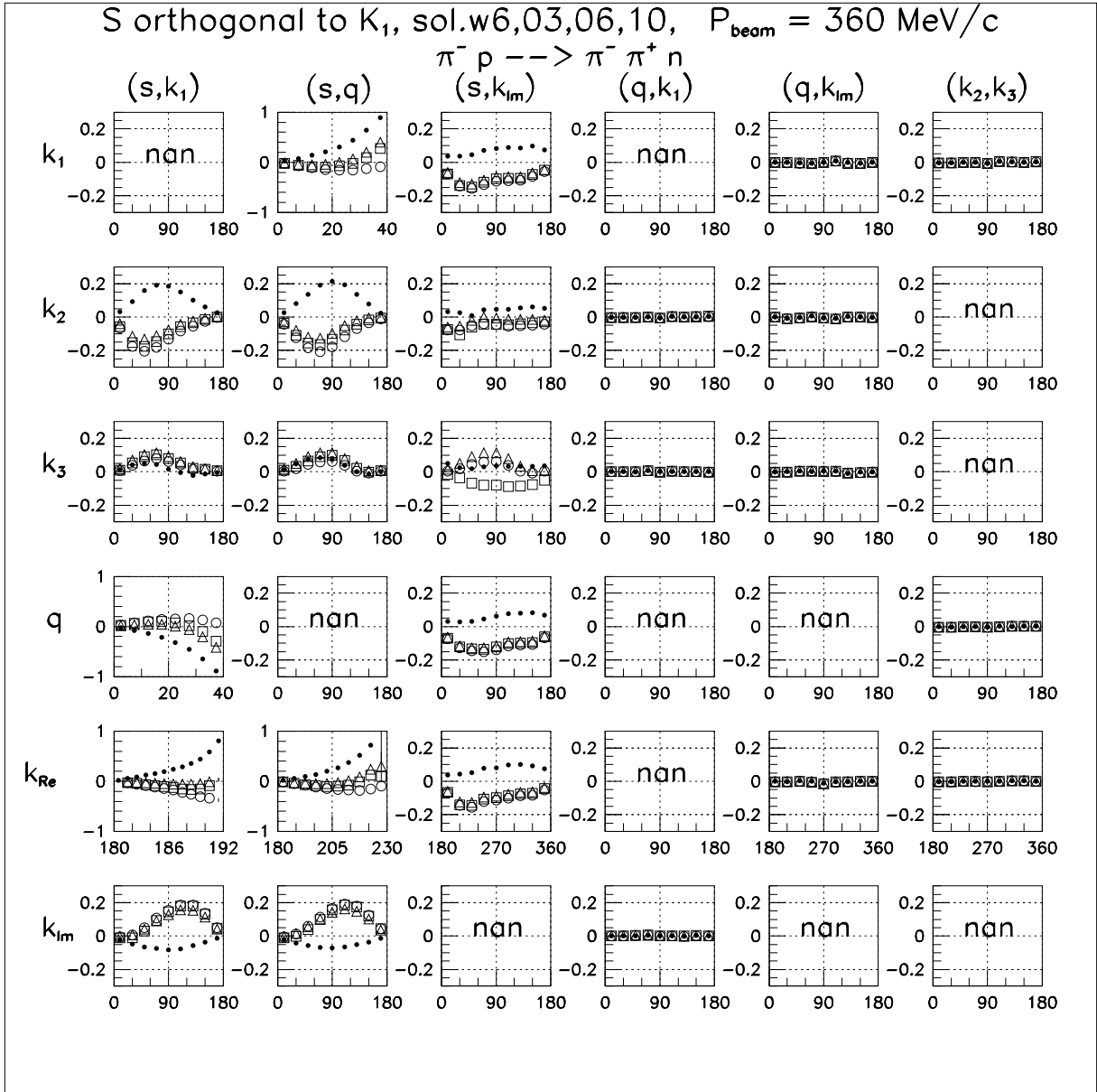


Figure 6: Asymmetries for the amplitudes sol06 (open circles), sol03 (open squares), sol10 (open triangles), solw6 (full dots) at  $(\mathbf{s} \perp \mathbf{k}_1)$  in the  $4\pi$ -steradian geometry device.